Journal of Power Sources, *28* (1989) 93 - 104

RESISTANCE OF EXPANDED GRIDS AND HIGH-RATE PLATE PERFORMANCE: PRELIMINARY RESULTS

E. M. VALERIOTE

Cominco Product Technology Centre, Sheridan Park, Mississauga, Ont., L5K 1B4 (Canada)

Introduction

The studies presented here on the resistance of expanded grids have been carried out in an effort to develop reliable and cost-effective methods for evaluating, or predicting, the effects of grid-design variables on plate performance in a lead/acid battery.

For grid resistance measurements, four degrees of approximation to a real battery system have been considered (Table 1). The resistance between the tab and the bottom bar of a grid has been taken as the zeroth approximation. This yields one number that gives an overall measure of the grid resistance, but under conditions far removed from the current density in a real plate. The first order of approximation is a widely used one in which a milliohmmeter is used to measure the resistance between the tab and individual points on the grid members, and a contour map of isoresistance points is developed. This is still unlike the current density in a real plate, but it was investigated in some detail because of its simplicity and popularity and because of its capability of identifying the distribution of conductivity across a plate. The latter distribution is important since, in a real plate, the current enters the grid over its entire face but accumulates and exits from

TABLE 1

Grid resistance measurements

Order of approximation	Procedure
0	Tab-to-bottom bar resistance far from real current density single number
1	Tab-point resistance contours still unlike real current density widely used 1-D profile
2	Isopotential contours: 1-D current enters uniformly across bottom of grid
3	Isopotential contours: 2-D current enters uniformly over face of plate no active material

0378-7753/89/$3.50

the tab only. In order to represent the true situation, a second order of approximation has been investigated in which the current enters the grid uniformly across its bottom bar rather than through a series of individual points as in the first-degree approximation. The isopotential contours, which are generated as a result of this current distribution, are measured and plotted similarly to the isoresistance contours developed earlier. The third order of approximation (Table 1) takes this process one step further by introducing the current uniformly over the face of the plate, although without active material in place, thereby coming still closer to reality. In the latter two approximations, the 1-D (one-dimension) and 2-D (two-dimension) refer not to the isopotential contours, but to the distribution of current entering the plate.

Finally, discharges of real plates with active material have been carried out at high rates, with reference electrodes placed at three points near the surface of the positive plate in order to monitor the potential distribution across the face of the place.

Results and discussion

First degree of approximation

Figure 1 shows the technique used to measure the grid resistance. Lines of constant resistance, with respect to a point on the tab, are obtained using an a.c. milliohmmeter in the four-terminal mode. The current (<50 μA) is applied between the top end of the tab and any selected point on the grid. The potential is measured between this latter point and the centre of the tab about 1 cm above the top bar. The map of constant resistance is then constructed by marking the points on a Xerox copy of the grid.

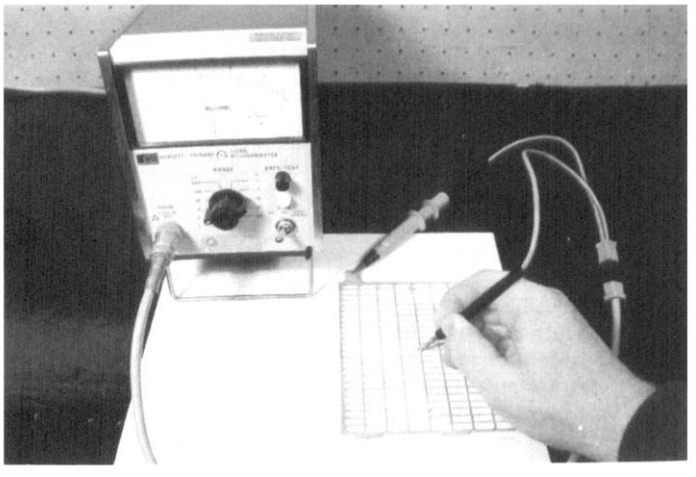

Fig. 1. Measurement of grid resistance using an a.c. milliohmmeter.

Typical isoresistance contours (1, 2, 3 and 4 mΩ) for book-mould grids of various designs are shown in Fig. 2. Because of the variation of heavy and light grid members, a very complicated contour is obtained if the measurements are made carefully. Similar measurements have been made for expanded grids (Fig. 3). The expanded grids have either a differential wire design (with members near the top of the grid being heavier than those at the bottom) or a constant-wire geometry (all wires have the same width). In addition, the grids have different top-bar heights or top-bar geometries.

Figure 4 gives resistance contours for other novel grid types including the so-called Cominco '3096 tooling' design. The latter is made with an extra fine mesh and has a constant-wire structure.

Second degree of approximation

Resistance data derived using the second degree of approximation method are presented in Fig. 5. In this case, the current is passed through the grid via the bottom bar, which is immersed in a mercury pool (Fig. 6) and potential differences are measured by a computer that senses the potentials through soldered leads (not shown in Fig. 6) at up to 25 grid points during the few seconds of current passage. The grids in Fig. 5(a) are both constant-wire designs but are made from different strip alloys. Figure 5(b), on the other hand, gives a comparison of a constant-wire-geometry grid (bottom, left) and a differential-wire-design grid (bottom, right). In both parts of Fig. 5, the isoresistance contours are shown, as before, as well as the equivalent resistances that are derived from the isopotential contours (heavy solid bands).

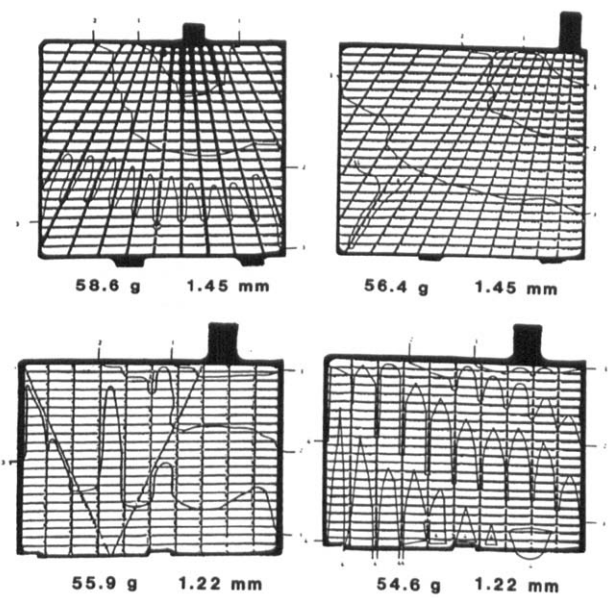

Fig. 2. Constant-resistance contours for book-mould cast grids. Grid weights and thicknesses are indicated.

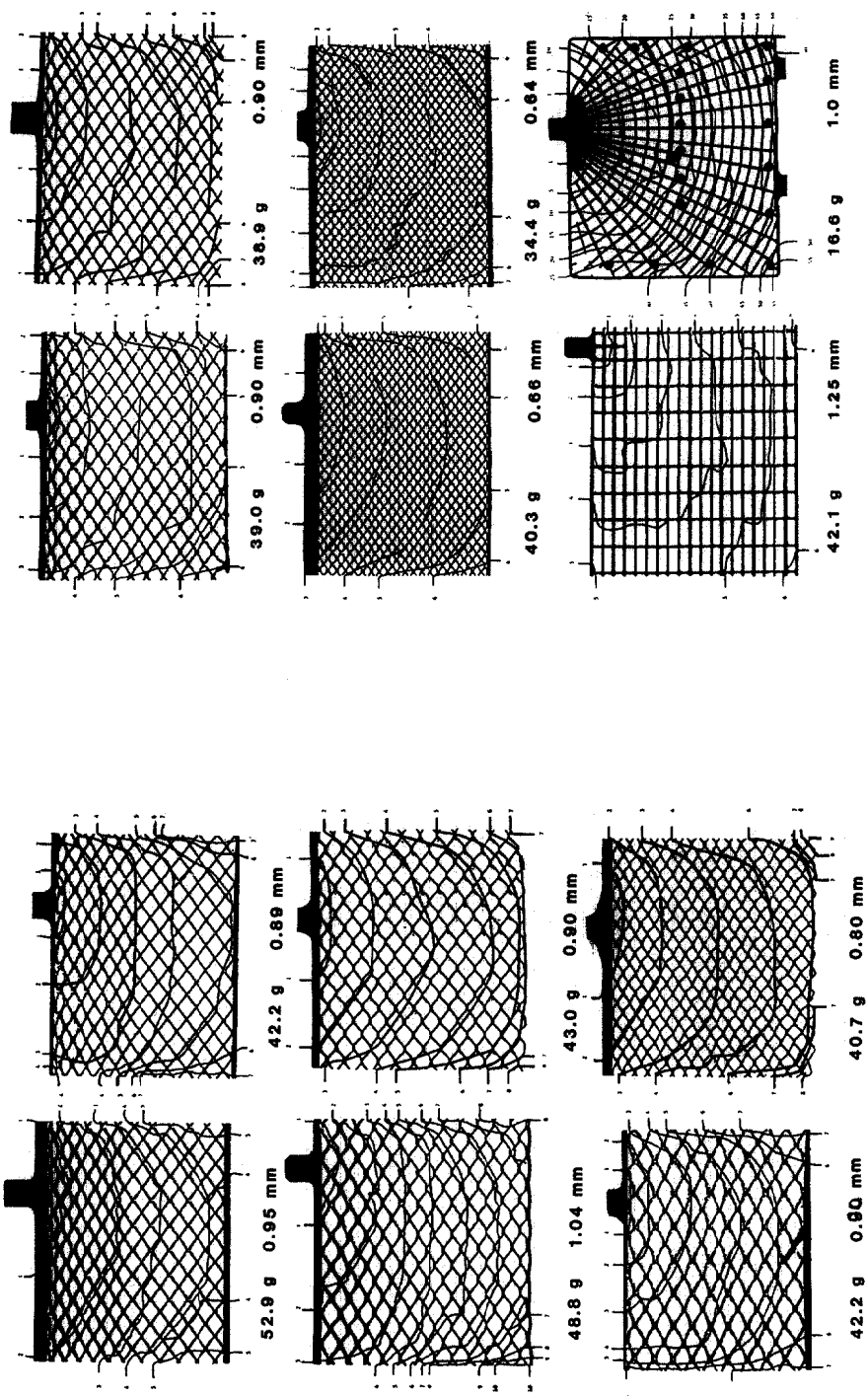

Fig. 3. Constant-resistance contours for expanded grids. Grid weights and thicknesses are indicated.

Fig. 4. Constant-resistance contours for expanded and novel grids. Grid weights are indicated, as well as strip or grid thicknesses.

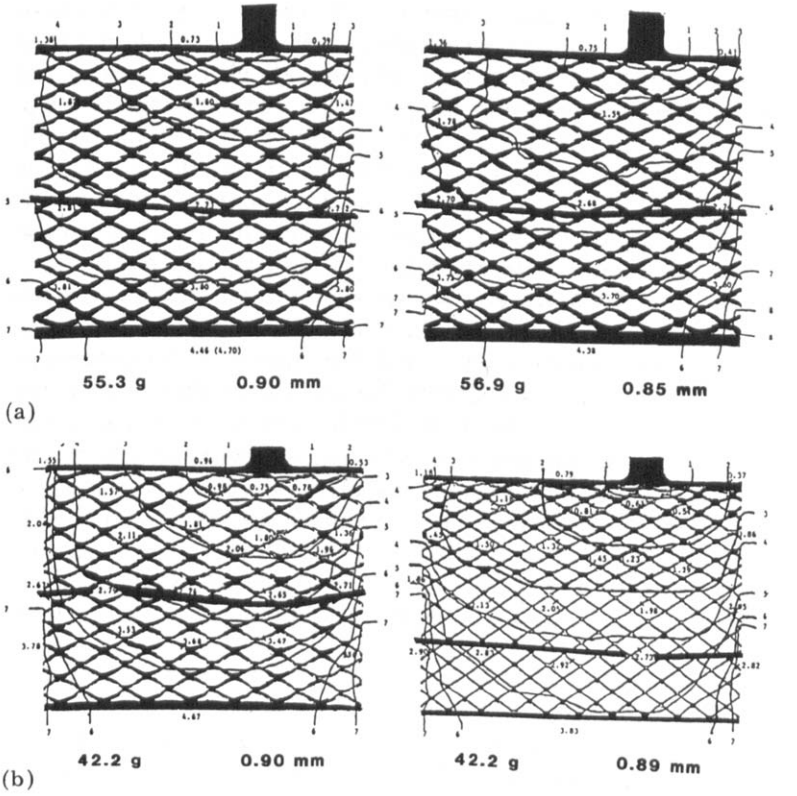

Fig. 5. Comparison of constant-resistance contours with polarizations (decimal numbers) per unit current obtained for grids with current applied uniformly across the width of the bottom bar. Heavy bands give approximate 2.75 mΩ isopotential (137.5 mV at 50 A) contours.

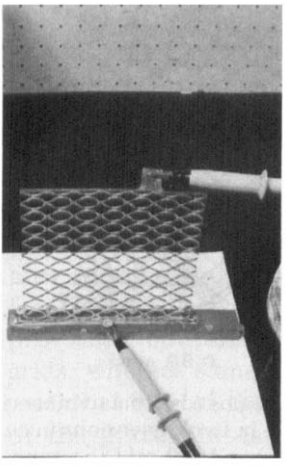

Fig. 6. Measurement of grid resistance using the second degree of approximation method (current passed through grid via the bottom bar).

For the two grids of the same design but different alloy (Fig. 5(a)), both the milliohm contours and the ispotential lines give almost identical results. As can be seen, the isopotential contours are much flatter than the milliohm contours and do not have the steeply rising edges obtained by the milliohmmeter method. The areas contained within the particular milliohmmeter contours are greater for the differential-wire design than for the constant-wire design (Fig. 5(b)). For example, the 3-mΩ contour for the differential design (bottom, right) extends almost halfway down the grid in the centre whereas it is much more restricted for the constant-wire geometry (bottom left). Similarly, the 2.75 mΩ equivalent isopotential (at 50 A) for the differential geometry is about two-thirds of the way down the grid, whereas, for the constant-wire design it is only about half way down. This experiment is more complicated to do, but it illustrates the distortion obtained by the less realistic milliohmmeter measurements at the edges of an expanded grid, or as would be the case for any grid without side members. With the milliohmmeter, the isoresistance contour rises very steeply near the edges, whereas the more realistic isopotential contour does not. Thus, with milliohmmeter measurements, care should be exercised in interpreting the steeply rising contours at the edges, particularly since the symmetrical components of these contours should be considered as artifacts of the method rather than as a simulation of the real behaviour of the grid.

Third degree of approximation

The results of experiments in which the current was passed over the entire surface of a grid immersed in an electrolyte cell (*i.e.*, third degree of approximation) are given in Fig. 7. As in Fig. 5(b), a constant-wire design (a) is compared with a differential-wire design (b) for grids of equal weight. Again, the isopotential contours are much flatter than contours obtained by

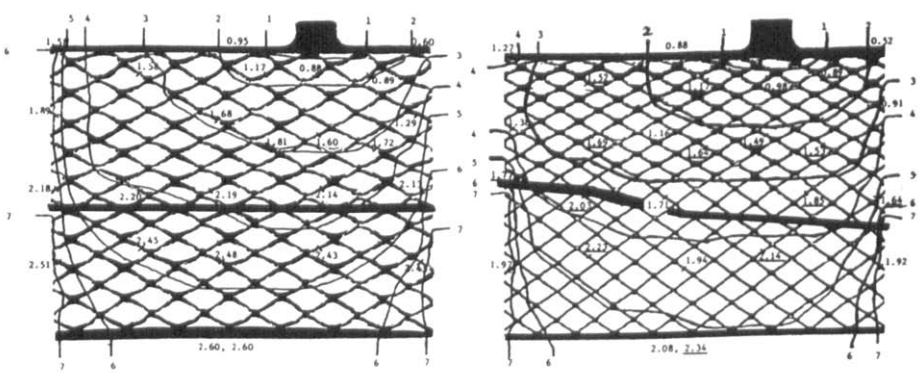

Fig. 7. Comparison of constant-resistance contours with polarizations (decimal numbers) per unit current obtained for grids with 50 A applied uniformly in two dimensions in an electrochemical cell. Heavy bands give approximate 2.25 mΩ (a) and 2.0 mΩ (b) isopotential contours at 50 A. The band for the right-hand grid was estimated assuming that the underlined isopotential values are correct.

the milliohmmeter method. Unlike those determined when current was passed into the bottom bar (second degree of approximation), the isopotential contours here are shown at about equal height, but have different equivalent resistance values. The equivalent resistance was ~2.25 mΩ for the constant-wire grid but only ~2.0 mΩ at the same height for the differential-wire grid.

High-rate discharge of pasted plates

Experiments using either the second or third degree of approximation are considerably more time-consuming and difficult to conduct than those using the milliohmmeter method to establish isoresistance contours. Apart from the above mentioned edge effects, the semi-quantitative information obtained is similar for all three methods. Accordingly, it would be convenient to be able to use the milliohmmeter method alone. To assess how data for the milliohmmeter measurements compare with real plate performance, high-rate discharge experiments were carried out on pasted plates contained in a specially designed cell. It should be emphasized that the results at this stage are very preliminary.

The reference electrodes were external to the cell but capillary probes entered the cell and monitored three points on the test electrode: (i) at the tab near the top bar; (ii) near the centre of the plate; (iii) at the bottom corner furthest from the tab. The reference electrode at the negative plate was positioned near the top of the plate, although this position was changed in later work. Automatic discharge/recharge was carried out under computer control at discharge rates of 100, 50, 5 A and, occasionally, at other rates up to 116 A. Since temperature was found to be a variable affecting the results, temperatures were monitored for each series of runs. In later experiments to those reported here, the temperatures were logged and used to automatically correct the computer-generated discharge capacity data. The discharge current was supplied by a computer-controlled electronic load, and recharge was by a programmable power supply.

Before discussing the results obtained using the above experimental setup, it is instructive to return to the isoresistance contours obtained by the milliohmmeter method to develop a definition of a grid 'figure of merit' in order to rank grids for comparison with their performance during polarization tests. In Fig. 8(a), the percentage of the grid area contained within a given resistance contour is shown as a function of the resistance for five grids (book-mould and expanded), each of approximately 60 g weight. The total area for all but one of these grids is contained within the 6 mΩ contour, and for four of the grids mostly within the 4 mΩ contour. The 3 mΩ contour provides a convenient point for comparison since it was included on all the grids, whereas some of the grids had no 4 mΩ contours. At 3 mΩ, it can be seen that 50% of the grid area is contained within the contour for all but one of the grids. The latter was an expanded grid with constant-wire geometry and had only 25% of its area within the 3 mΩ contour. Similar area/contour comparisons were made for lower ranges of grid weight, *i.e.*, 49 - 56 g grids

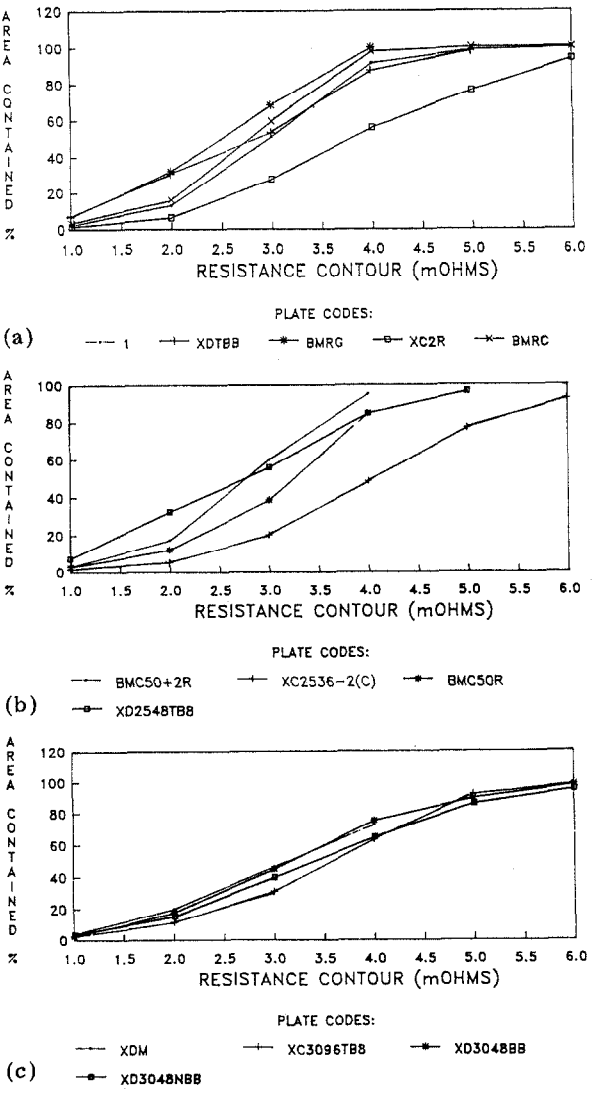

Fig. 8. Area (%) within resistance contour. Grid weight: (a) 56 - 63 g; (b) 49 - 56 g; (c) 34 - 40 g.

(Fig. 8(b)) down to very light grids (34 - 40 g) that included some with very fine mesh (Fig. 8(c)) but book-mould types this light were unavailable.

A figure of merit (*FOM*) was defined both for absolute and relative grid areas. The absolute *FOM* was defined as the grid weight (expressed in g) multiplied by the area (in cm^2) within the resistance contour and divided by the value of that resistance (in $m\Omega$). Similarly, a relative *FOM* was calculated, using the relative contained area, with the only difference being that the enclosed area was defined as a percentage of the total area, rather than as an absolute value. Table 2 shows figures of merit for 4 grids. The XDII and

TABLE 2

Ranking of grids (3 mΩ contours)

Grid code	Figure of merit (*FOM*)	
	Absolute	Relative
XDII	1088	634
XDM	1070	631
XDTB2	852	542
XC	452	289

XDM grids were taken from commercially available batteries and had a differential-wire expanded design. The XDTB2 grid was an experimental differential-wire design and had a top bar 2 mm in height. The XC grid was one of similar weight to the other three but differed in having a constant-wire cross section. Each *FOM* value in Table 2 was based on the 3 mΩ contour line. The grid ranking was then compared with performance under the plate polarization test.

Figure 9(a) shows plate potentials as a function of time during a 100 A discharge of a single plate having a constant-wire expanded-grid geometry. The lower three curves are the plate potentials measured with respect to each of the three reference electrodes. As can be seen, there is less polarization with respect to the reference electrode near the tab than that near the centre or bottom of the plate. The upper curve is a measure of the overall cell potential difference with the ohmic drop across the electrolyte subtracted, in order to simulate the voltage that would be observed in a real battery. Although there is a one-inch spacing between the test and counter electrodes, only the electrolyte in the immediate vicinity of the plates is utilized under such high-rate discharge conditions. Thus, by subtracting the potential drop across that electrolyte, the values obtained should be very similar to what would be measured for the corresponding current per plate in a real battery. Similar results were obtained for the differential-wire-geometry experimental grids (Fig. 9(b)), although in this case the plate potential measured with respect to the tab crosses over the values recorded at the centre and bottom of the plate and then declines rather quickly. This behaviour is reflected in the overall cell potential (*cf.* upper curve) and was related to the positioning of the reference electrodes near the tab for both positive and negative plates, together with the convection that occurs as a result of the water and heat produced during the discharge (see following discussion). As was decided later, it is more desirable to use the reference electrode near the plate centre in order to compare one plate with another. Finally, Fig. 9(c) shows typical curves for one of the commercial grids (XDM). A potential minimum was usually observed near 3 s followed by a slight maximum. The potential minimum may have been caused by nucleation overvoltage or by water production (see below).

With the cell design used in the above experiments, it was possible to observe the test plate through the end of the cell during the discharge.

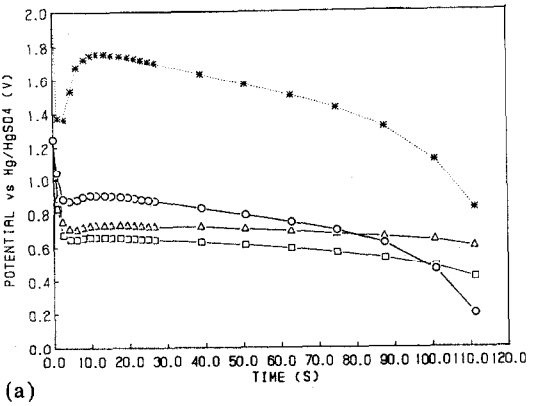

(a)

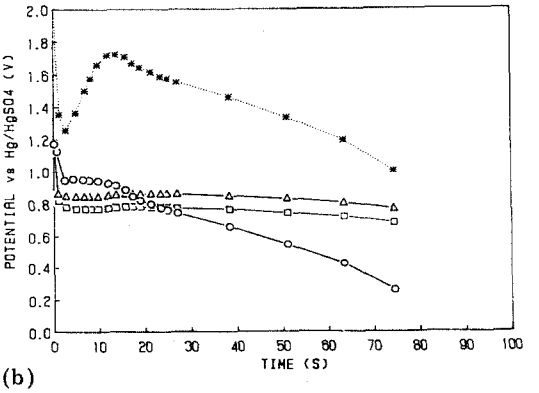

(b)

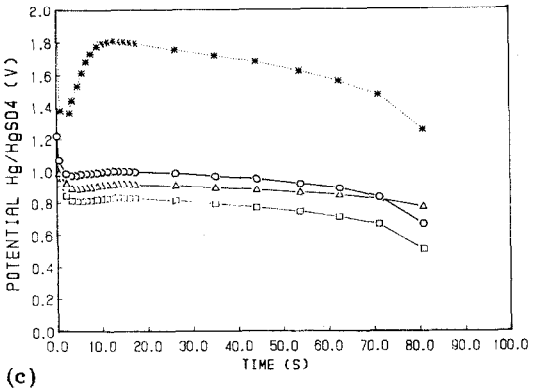

(c)

Fig. 9. Polarization of battery plates during 100 A discharge: (a) constant-wire expanded grid (42.4 g, code XC); (b) differential-wire expanded grid (42.5 g, code XDTB2); (c) commercial expanded grid (40.7 g, code XDM). Plate potential *vs.* reference capillary near: (○) tab; (△) centre; (□) bottom. Upper curve (*) in each plots is *iR*-corrected cell potential.

Within about 3 s of the initiation of a 100 A discharge, *i.e.*, near the potential minimum (Fig. 9), glassy-like islands began to appear on the surface when viewed at a glancing angle. The areas covered by this mirror-like coating increased until, at 10 - 15 s, the entire plate had the appearance of a freshly-created skating surface. Within 1 min, variations in the index of refraction, within 1 to 2 mm of the surface of the plate, indicated upward streaming of the electrolyte. Towards the end of the discharge, or sometimes not until the open-circuit period following the discharge, a fine light gassing began, with the gas bubbles entrained in the upward stream. Even after over 5 min on open-circuit, the mirror-like surface had not completely disappeared. When a subsequent charge was begun at ~10 A, however, the mirror partially disappeared within 15 to 30 s, and completely disappeared within 1 to 2 min. Very similar observations were made for 50 A discharges, except that the progression of the mirror-like surface took twice as long as at 100 A. Thus, the convection caused by water production could be observed directly.

At high current densities, the current is collected over the entire grid but can only exit from the plate through the tab area. As a result, a very high degree of local heating is observed near the tab; this also contributes to the convective effect. Since the greatest disturbances are near the tab, it was decided, as mentioned above, that the reference electrode near the plate centre was more reliable than that near the tab for making plate comparisons.

If the polarization of the plates (Fig. 9) is compared with the calculated figures of merit (Table 2), using the centre reference electrode, it can be seen, Fig. 10, that the polarization during a 100 A discharge of the constant-wire-geometry expanded electrode (XC) is considerably greater than that of the three differential-wire designs. The figures of merit given in Table 2 indicate that the XDII and XDM plates should exhibit similar performance, that the XDTB2 plate should be somewhat poorer, and that the XC plate

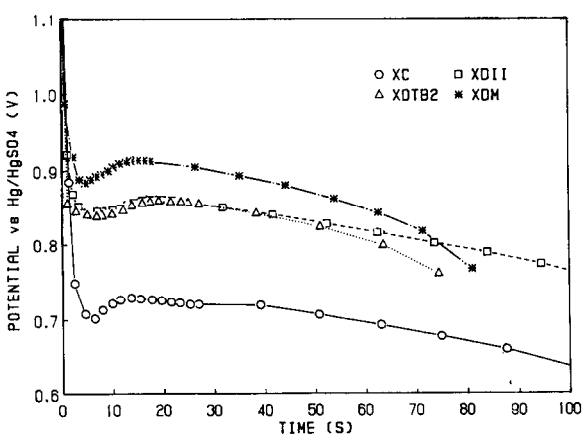

Fig. 10. Comparison of discharges at 100 A for plates with expanded grids.

should be substantially poorer. The polarization data of Fig. 10 is in qualitative agreement with these predictions.

As emphasized previously, these studies are preliminary. Nevertheless, there does seem to be promise of useful results. In part, the discrepancies were probably related to the degree of reproducibility that could be obtained at the time of carrying out the high-rate discharge experiments. The cell design has since been modified and control of the experimental conditions has been enhanced in order to improve the reproducibility. With these developments, it will be possible to repeat the experiments reported here and determine whether the present figures of merit have sufficient precision, or whether they can be refined and their predictive value improved.

Conclusions

Despite being obtained under conditions only crudely approximating the real current distribution in battery plates, milliohmmeter-determined resistance measurements are useful in predicting relative plate performance. However, the steeply rising resistance contours at the grid edges are artefacts and should not be given much importance.

The calculated 'figure of merit', based on resistance contours, has also proved useful. Nevertheless, more detailed study is required to determine whether it is the best function to define and how accurately it provides predictions of plate performance. Such work will be reported in a future communication.

Acknowledgement

The author would like to express his appreciation to David A. J. Rand for exercising excellent editorial judgement in converting the verbal presentation to this published paper.